ARTICLE

Topological quantum chemistry

Barry Bradlyn[1]*, L. Elcoro[2]*, Jennifer Cano[1]*, M. G. Vergniory[3,4,5]*, Zhijun Wang[6]*, C. Felser[7], M. I. Aroyo[2] & B. Andrei Bernevig[3,6,8,9]

Since the discovery of topological insulators and semimetals, there has been much research into predicting and experimentally discovering distinct classes of these materials, in which the topology of electronic states leads to robust surface states and electromagnetic responses. This apparent success, however, masks a fundamental shortcoming: topological insulators represent only a few hundred of the 200,000 stoichiometric compounds in material databases. However, it is unclear whether this low number is indicative of the esoteric nature of topological insulators or of a fundamental problem with the current approaches to finding them. Here we propose a complete electronic band theory, which builds on the conventional band theory of electrons, highlighting the link between the topology and local chemical bonding. This theory of topological quantum chemistry provides a description of the universal (across materials), global properties of all possible band structures and (weakly correlated) materials, consisting of a graph–theoretic description of momentum (reciprocal) space and a complementary group–theoretic description in real space. For all 230 crystal symmetry groups, we classify the possible band structures that arise from local atomic orbitals, and show which are topologically non–trivial. Our electronic band theory sheds new light on known topological insulators, and can be used to predict many more.

For the past century, chemists and physicists have advocated fundamentally different perspectives on materials: chemists have adopted an intuitive 'local' viewpoint of hybridization, ionic chemical bonding and finite-range interactions, whereas physicists have described materials through band structures or Fermi surfaces in a non-local, momentum-space picture. These two descriptions seem disjoint, especially with the advent of topological insulators, which are exclusively understood in terms of the non-trivial topology of Bloch Hamiltonians throughout the Brillouin zone in momentum space. Despite the apparent success in predicting some (mostly time-reversal-invariant) topological insulators, conventional band theory is ill-suited to their natural treatment. Given the paucity of known topological insulators (fewer than 400 materials out of the 200,000 existent in crystal structure databases), one may ask whether topological materials are truly so rare, or if this reflects a failing of the conventional theory.

The topological properties of energy bands are intrinsically global in momentum space. The duality between real and momentum (direct and reciprocal) space suggests that the properties of bands that are non-local in momentum space will manifest locally in real space. Here we unify the real- and momentum-space descriptions of solids, to provide a powerful, complete and predictive band theory. Our procedure provides a complete understanding of the structure of energy bands in a material, and links the topological properties of the material to the chemical orbitals at the Fermi level. It is therefore a theory of topological quantum chemistry.

We develop the complete theory of topological bands in two main steps. First, we compile all of the possible ways energy bands in a solid can be connected throughout the Brillouin zone to obtain all realizable band structures in all non-magnetic space groups. Crystal symmetries place strong constraints on the allowed connections of bands. At high-symmetry points (k_i) in the Brillouin zone, Bloch functions are classified by irreducible representations of the symmetry group of k_i, which also determine the degeneracy. Away from these high-symmetry points, fewer symmetry constraints exist and some degeneracies are lowered. This result is central to the $k \cdot p$ approach[1] to band structure,

which provides a good description nearby the high-symmetry k_i points. However, to determine the global band structure, the different $k \cdot p$ expansions about each k_i need to be patched together. Group theory places constraints—'compatibility relations'—on how this can be done. Each solution to these compatibility relations gives groups of bands with different connectivities, corresponding to different physically realizable phases of matter (trivial or topological). We solve all of the compatibility relations for all 230 space groups by mapping connectivity in band theory to the graph-theoretic problem of constructing multipartite graphs. Classifying the allowed connectivities of energy bands becomes a combinatorial problem of graph enumeration: we present a fully tractable, algorithmic solution.

Second, we develop the tools to compute the way in which the real-space orbitals in a material determine the symmetry character of the electronic bands. Given only the Wyckoff positions and the orbital symmetry (s, p, d and so on) of the elements or orbitals in a material, we derive the symmetry character of all of the energy bands at all points in the Brillouin zone. We do this by extending the notion of a band representation, first introduced in refs 2 and 3, to the physically relevant case of materials with spin–orbit coupling (SOC) and/or time-reversal symmetry. A band representation consists of all energy bands (and Bloch functions) that arise from localized orbitals respecting the crystal symmetry (and possibly time-reversal symmetry). The set of band representations is strictly smaller than the set of groups of bands obtained from our graph theory[4]. We identify a special subset of 'elementary' band representations (EBRs)[2,5], elaborated on in Supplementary Information, which correspond to the smallest sets of bands that can be derived from localized atomic-like Wannier functions[6]. The 10,403 different EBRs for all of the space groups, Wyckoff positions and orbitals are presented in ref. 7.

If the number of electrons is a fraction of the number of connected bands (connectivity) that form an EBR, then the system is a symmetry-enforced semimetal. The EBR method allows us to easily identify candidate semimetallic materials. We find that the largest possible number of connected bands in an EBR is 24 and hence the smallest

possible fraction of filled bands in a semimetal is 1/24. If, however, our graph analysis reveals an instance for which the number of connected bands is smaller than the total number of bands in the EBR, then we conclude that a momentum-space (k-space) description exists but a Wannier one does not[8–10], that is, the disconnected bands are topological. Topological insulators are thus those materials with bands that are not in our list of elementary components but that are in our graph enumeration. We therefore reformulate the momentum-space approach to topological indices in terms of obstructions in real space to the existence of atomic-like Wannier functions. In tandem with our graph-theoretic analysis of band connectivity, we enumerate all of the ways the transition to a topological phase can occur. Hence, we are able to classify all topological crystalline insulators. This classification leads to previously unrecognized, large classes of topological insulators. We demonstrate the power of our approach by predicting hundreds of new topological insulators and semimetals.

Graph theory and band structure

To construct a band theory that accounts for the global momentum-space structure of energy bands, we piece together groups of bands from distinct points in the Brillouin zone. Consider a D-dimensional crystalline material that is invariant under the action of a space group G, containing elements of the form $\{R|d\}$, where R is a rotation or rotoinversion, d is a translation and we use the notation that, acting on coordinates, $\{R|d\}x = Rx + d$. Each space group contains a Bravais lattice of translations is generated by a set of linearly independent translations $\{E|t_i\}$, $i = 1, …, D$, where E represents the identity. Each k in the Brillouin zone remains invariant (up to a translation by a reciprocal lattice vector) under the action of the symmetry elements in its little group $G_k \subset G$, and the Bloch wavefunctions $|u_n(k)\rangle$ transform under a sum of irreducible representations of G_k; bands at high-symmetry k points will have (non-accidental) degeneracies equal to the dimension of these representations. For spinless systems and systems without SOC, these representations are ordinary linear representations; for systems with SOC, they are double-valued representations. Away from high-symmetry points, degeneracies are reduced and bands disperse according to conventional $k \cdot p$ theory.

Consider two different high-symmetry k points, k_1 and k_2, and a line $k_t = k_1 + t(k_2 - k_1)$ parameterized by $t \in [0, 1]$ connecting them. To determine how the irreducible representations at k_1 connect to those at k_2 to form bands along this line, we note that the little group G_{k_t} at any k_t on the line is a subgroup of both G_{k_1} and G_{k_2}. Therefore, an irreducible representation ρ of G_{k_1} at k_1 will split (or, formally, restrict or subduce) along the line to a (direct) sum of irreducible representations $\bigoplus_i \tau_i$ of G_{k_t}. Using $\downarrow$ to denote restriction, we write

$$\rho \downarrow G_{k_t} \approx \bigoplus_i \tau_i \tag{1}$$

(here and throughout we use "$\approx$" to denote equivalence of representations). These restrictions are referred to as compatibility relations. Heuristically, they are found by taking the representation ρ and 'forgetting' about the symmetry elements of G_{k_1} that are not in G_{k_t}. Because energy bands in a crystal are periodic, the representations σ of G_{k_2} at k_2 must also satisfy $\sigma \downarrow G_{k_t} \approx \bigoplus_i \tau_i$. Each representation τ_i corresponds to a (group of) band(s) along the line k_t; bands coming from k_1 in each irreducible representation τ_i must join with a group of bands coming from k_2 that transform in the same irreducible representation. We refer to each set of such pairings as a solution to the compatibility relations.

Compatibility relations apply to each and every connection line or plane between each pair of k points in the Brillouin zone, leading to strong but factorially redundant restrictions on the number of bands that can connect in a crystal. To construct the non-redundant solutions to the compatibility relations, we map the question to a problem in graph theory. Each irreducible representation at distinct k points unrelated by symmetry labels a node in a graph. In our previous example, the nodes would be labelled by ρ, σ and $\{\tau_1, \tau_2, …\}$ for the k_1, k_2 and k_t

high-symmetry points and line, respectively. We draw the edges of the graph using the following rules: (i) irreducible representations at the same k can never be connected by edges (our graph is multipartite); (ii) nodes that correspond to irreducible representations at k_a and k_b can be connected only if $G_{k_a} \subseteq G_{k_b}$ or $G_{k_b} \subseteq G_{k_a}$ (that is, k vectors are compatible); and (iii) edges must be consistent with the compatibility relations. For instance, equation (1) corresponds to an edge from the node labelled by ρ to each node labelled by τ_i. We refer to such a graph as a connectivity graph.

We developed an algorithm (described in Supplementary Information) that outputs all distinct connectivity graphs for all space groups—a very computationally intensive task. The factorial complexity is handled by several subroutines, which ensure that the minimal set of paths in momentum space is considered. Additional filters remove redundant or isomorphic solutions to the compatibility relations. The tools of graph theory then enable us to partition the nodes of the graph (the little-group irreducible representations) into distinct connected components (subgraphs). Each component corresponds to a connected, isolated group of bands that can describe a set of valence bands in some insulating system or protected semimetal, depending on the filling. In particular, such a list consists of all (both topologically trivial and non-trivial) valence-band groups. The familiar example of graphene with SOC is given in Fig. 1 and Supplementary Information. We now define and classify topologically non-trivial bands in terms of localized Wannier functions.

Topologically (non–)trivial bands

Consider a group of connected bands in the spectrum of a crystal Hamiltonian separated by a gap from all others. Using existing machinery, determining whether this group is topologically non-trivial requires discovering topological invariants (indices or Wilson loops) from the analytic structure of the Bloch eigenfunctions. We now prove that the algebraic global structure of the energy spectrum itself (including connectivities) contains a complete classification of topological materials. We define:

Definition 1

An insulator (or, more generally, a filled group of bands) is topologically non-trivial if it cannot be continued to any atomic limit without either closing a gap or breaking a symmetry.

We associate a set of Wannier functions—orbitals obtained by Fourier transforming linear combinations of the Bloch wavefunctions—with every isolated group of energy bands. In an atomic limit, the Wannier functions are exponentially localized, respect the symmetries of the crystal (and possibly time-reversal) and coincide in most cases (however, see section 'Hybridization, bonds and obstructed atomic limits') with the exponentially localized atomic orbitals at infinite (atomic limit) separation. Under the action of the crystal symmetries, different atomic sites are distributed into orbits, which correspond to Wyckoff positions; we denote the points in a Wyckoff orbit in a unit cell as $\{q_i\}$. In analogy with the symmetry group of a k point, for each site q_i there is a finite subgroup G_{q_i} of the full space group G that leaves q_i invariant; this subgroup is called the site-symmetry group. For example, the A and B sites in graphene belong to Wyckoff position $2b$ (the multiplicity 2 refers to the number of symmetry-related sites in the unit cell); its site-symmetry group is isomorphic to C_{3v}. Wannier functions at each site q_i transform under some representation ρ_i of G_{q_i}. Crucially, through the mathematical procedure of induction, the real-space transformation properties of these localized Wannier functions determine the little-group representations of the bands at every point in the Brillouin zone: the action of the space group on the full lattice (rather than just the unit cell) of Wannier functions gives an infinite-dimensional representation. The Fourier transform of this representation gives the k-dependent matrix representation of all symmetry elements. This respresentation can then be restricted to representations
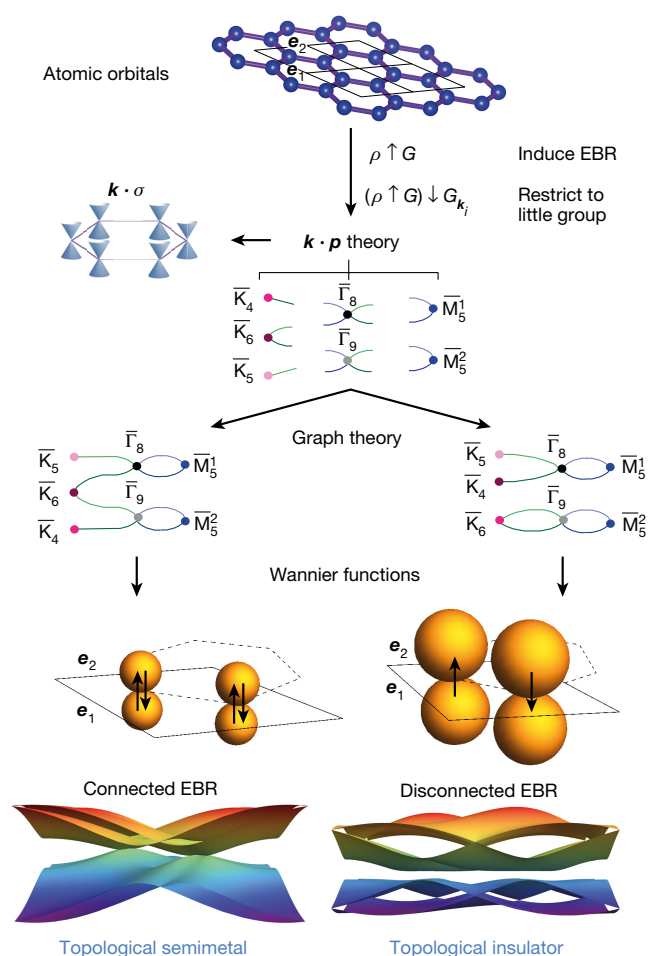
Figure 1 | Schematic of theory applied to graphene with SOC. We begin by inputting the orbitals ($|p_z \uparrow\rangle$ and $|p_z \downarrow\rangle$) and lattice positions (the blue spheres in the honeycomb lattice defined by Bravais lattice vectors e_1 and e_2) that are relevant near the Fermi level. Following the first arrow, we then induce an EBR $\rho \uparrow G$ from these orbitals, which restricts to little-group representations $(\rho \uparrow G) \downarrow G_{k_i}$ at the high-symmetry points $k_i = \Gamma$, M and K in the Brillouin, shown here as nodes in a graph and labelled according to the notation used by the Bilbao Crystallographic Server[7]. Standard $k \cdot p$ theory allows us to deduce the symmetry and degeneracy of energy bands in a small neighbourhood of these points, indicated by the different coloured edges emanating from the nodes. This leads to the low-energy $k \cdot \sigma$ dispersion shown to the left, where σ is the vector of 2×2 Pauli matrices. The graph-theory mapping enables us to solve the compatibility relations along these lines in two topologically distinct ways. On the left, we obtain a graph with one connected component, indicating that in this phase graphene is a symmetry-protected topological semimetal. The Wannier functions for the four connected bands coincide with the atomic-orbial Wannier functions (yellow spheres, with spins indicated by arrows), leading to a gapless semimetallic dispersion (bottom left). In contrast, the graph on the right has two disconnected components, corresponding to the topological insulator phase of graphene by Definition 1. The spin-up and spin-down localized Wannier functions for the valence band are localized on distinct sites of the hexagonal lattice, and so break time-reversal symmetry in real space[8]. This leads to a topologically gapped band structure (bottom right).

of the little group of each k. Following ref. 2, we refer to this infinite-dimensional representation as a band representation ρ_{iG} induced[11] in the space group G by the representation ρ_i of G_{q_i}: $\rho_{iG} \equiv \rho_i \uparrow G$. This definition can be applied with or without time-reversal symmetry. Band representations that also respect time-reversal symmetry in real space are physical band representations (PBRs).

By inducing band representations, we enumerate all groups of bands with exponentially localized and symmetric Wannier functions. Each

such group forms a band representation, and every band representation is a sum of EBRs. We identified all of the 10,403 EBRs:

Proposition 1

A band representation ρ_G is elementary if and only if it can be induced from an irreducible representation ρ of a maximal (as a subgroup of the space group; see Supplementary Information) site-symmetry group G_q that does not appear in a list of exceptions[4,12] given in Supplementary Information.

We prove a similar statement for physical elementary band representations (PEBRs) and determine the extensive list of exceptions[7]. In analogy with irreducible representations, a (P)EBR cannot be written as a direct sum of other (P)BRs. A band representation that is not elementary is a 'composite' band representation (CBR). Crucially, Definition 1 implies that any topologically trivial group of bands is equivalent to some (physical, if time-reversal symmetry is unbroken) band representation. Conversely, any topologically non-trivial group of bands cannot be equivalent to any of the enumerated band representations, physical or otherwise (a caveat is discussed in section 'Hybridization, bonds and obstructed atomic limits').

We therefore conclude that the Wannier functions of a topologically trivial group of bands are smoothly continuable into an atomic limit, are exponentially localized and transform under a band representation. In a topological material, the Wannier functions for the valence (group of) bands either fail to be exponentially localizable or break the crystal symmetry. An example of the former is the Chern insulator: a non-vanishing Chern number indicates an obstruction to the formation of exponentially localized Wannier functions[13]. The Kane–Mele model of graphene[14] (see section 'Classification of topological insulators') is an example of the latter: in the Z_2 non-trivial phase, exponentially localized Wannier functions for the valence bands necessarily break time-reversal symmetry[8] (when the valence and conduction bands are taken together, atomic-like Wannier functions can be formed). Hence, to transition to the atomic limit a gap must close.

We tabulated all of the EBRs and PEBRs induced from every maximal Wyckoff position (that is, a Wyckoff position with maximal site-symmetry group) for all 230 space groups, with and without SOC and/or time-reversal symmetry. These data enable us to enumerate all topologically trivial band structures. In an accompanying publication[7] we describe the group-theoretic data (subduction tables, and so on) for each of the 5,646 EBRs and 4,757 PEBRs that we find. To generate these data, we generalized the well-known induction algorithm based on Frobenius reciprocity[5,15] to the case of double-valued representations; see ref. 7 for full details of the computational methods. The group-theoretic data and the full set of EBRs and PEBRs can be accessed through programs hosted on the Bilbao Crystallographic Server (http://www.cryst.ehu.es/cgi-bin/cryst/programs/bandrep.pl); we provide a summary table of all of the EBRs and PEBRs in Supplementary Information section VII.

Our approach provides a classification of topological insulators that is both descriptive and predictive. Rather than provide a classification (for example with a topological index) of the topological phases in each space group, we instead formulate a procedure to determine whether a band structure is topologically trivial or non-trivial, and enumerate the possible non-trivial band structures for each space group. Given the band structure of a material, we can compare isolated energy bands to our tabulated list of EBRs and PEBRs. Any group of bands that transforms as a EBR or PEBR is topologically trivial. Those groups of bands that remain are guaranteed to be topologically non-trivial. Conversely, knowing only the valence orbitals and crystal structure of a material, we can immediately determine under which (if any) EBRs the bands near the Fermi level transform. If graph theory reveals that these EBRs can be disconnected, then we deduce that the phase is topological. Although a disconnected EBR itself serves as a topological

index, standard techniques can be used to diagnose which (if any) of the more standard K-theoretic topological indices[16] are non-trivial. In the subsequent sections, we outline this method and present hundreds of newly predicted topological materials.

Our identification of topological crystalline phases also goes beyond recently proposed classifications[17] based on symmetry eigenvalues of occupied bands in momentum space, which were subsequently applied in a modified form to three-dimensional systems[18]. A shortcoming common to both methods is that, although they produce a list of topological indices for each space group, they provide no insight into how to find or engineer materials in any non-trivial class. In addition, in contrast to the claims of ref. 18, by focusing only on eigenvalues in momentum space rather than the real-space structure of Wannier functions (or equivalently, the analytic structure of Bloch functions in momentum space), essential information about the topological properties of certain band structures is lost. For instance, the topological phases of space group $P6mm$ (number 183; see Supplementary Information) fall outside the scope of ref. 18. Viewed in this light, our classification based on band representations generalizes the notion of a topological eigenvalue invariant in such a way as to capture these missing cases.

Classification of topological insulators

Combining the notion of a band representation with the connectivity graphs, we identify two broad classes of topological insulator, distinguished by the number of relevant EBRs at the Fermi level when transitioning from a topologically trivial to non-trivial phase. For the first class, if in a trivial phase the Fermi level sits in a single EBR or PEBR, then the material is necessarily a semimetal. If tuning an external control parameter (such as strain or SOC) opens a gap at the Fermi level, then the material necessarily becomes topological. This is because, if a (P)EBR splits into a disconnected valence and conduction band, then neither the valence nor the conduction band can form band representations; only both together form a (P)EBR. A material in the first class thus occurs exactly when an EBR can be consistently realized in a disconnected way in the Brillouin zone. We can determine when this is possible using the machinery introduced in section 'Graph theory and band structure'. The archetypal example of this behaviour is the quantum spin Hall transition in the Kane–Mele model of graphene with both next nearest-neighbour 'Haldane'[19] and Rashba SOC (Fig. 1). This model hosts two spinful p orbitals per hexagonal unit cell, for a total of four bands forming an EBR. In the Rashba SOC regime, all four bands are connected and the material is a gapless semimetal. Increasing the Haldane SOC opens a band gap. By the preceding analysis, this gap must be topological. We tabulate all (hundreds of) EBRs and PEBRs—each specified by an orbital, Wyckoff position and space group—in which such a topological gap can occur in the BANDREP program on the Bilbao Crsystallographic Server (http://www.cryst.ehu.es/cgi-bin/cryst/programs/bandrep.pl), described in ref. 7; see Supplementary Information for full details.

The second class of topological insulator is defined by the presence of more than one relevant EBR at the Fermi level. The trivial phase of such a material can be an insulator, with EBRs above and below the Fermi level. Without loss of generality, we consider one EBR in the conduction band and one in the valence band; generically, any transition involving more than two EBRs can be resolved into a sequence of pairwise transitions. A topological phase transition occurs when a gap closes and reopens after a band inversion, such that neither the valence bands nor the conduction bands form a band representation. In the trivial phase, the little-group irreducible representations of the filled bands at each $\boldsymbol{k}$ are those of the EBR of the valence bands. After the topological phase transition, the little-group irreducible representations at each $\boldsymbol{k}$ are not consistent with an EBR. This mechanism describes the three-dimensional topological insulator Bi_2Se_3 (refs 20, 21). Without, or with very small, SOC, Bi_2Se_3 is a trivial insulator: its valence and conduction bands transform in two distinct EBRs. Increasing the SOC pushes the

Table 1 | Summary of topological phase transitions

Number of PEBRs without SOC	Number of PEBRs with SOC	Examples
1	1	Graphene, bismuthene, Cu_3SbS_4
1	2	Bi^{1-} square nets, $Cu_2SnHgSe_4$
2	2	Bi_2Se_3, KHgSb

The topological phase transitions are between a system without SOC to a topological insulator with SOC, for band representations induced from up to two irreducible representations of the site-symmetry group of occupied Wyckoff positions. The first column gives the number of PEBRs that directly straddle the Fermi level without SOC (per spin). The second column shows how this number of band representations changes when SOC is turned on. When there is a single PEBR in the first column, the system is necessarily a semimetal without SOC; these materials become topological insulators for arbitrarily small SOC.

bands together; at a critical SOC strength, the gap between the valence and conduction bands closes at the Γ point of the Brillouin zone. Above this critical value a gap reopens, with certain states (labelled by irreducible representations of G_Γ) exchanged between the valence and conduction bands. Ultimately, neither the valence bands nor the conduction bands transform as EBRs and the insulator is topological[22] as per Definition 1. If, on the other hand, we consider a hypothetical material in which a full gap does not reopen after band inversion, it will instead be a symmetry-protected semimetal, similar to Cd_3As_2 (ref. 23) or Na_3Bi (ref. 24).

When the phase transition is driven by SOC we label the classes by (n, m), where n is the number of EBRs at the Fermi level in the trivial phase (without SOC) and m is the number in the topological phases (after SOC is turned on). These phases are indicated in Table 1, along with material examples.

To summarize the theoretical results: we first showed that the constraints placed by group theory in momentum space on the allowed connectivity of bands can be solved via a mapping to graphs. We constructed all of the possible allowed, isolated band groupings for all 230 space groups. We then showed that our group-theoretic analysis in real-space determines—through the notion of band representations—which of these isolated band groups are described by localized, symmetric Wannier functions (corresponding to topologically trivial insulators). It follows that any other group of valence bands in an insulator necessarily constistute a topological insulator. Our theory also shows that there are different classes of topologically trivial insulator, which cannot be adiabatically continued to one another. We now link this important fact to orbital hybridization.

Hybridization, bonds and obstructed atomic limits

Given a topologically trivial crystal, it is tempting—but wrong—to assume that the electronic Wannier functions, like the constituent atomic orbitals, are localized at the atomic positions. Orbitals from different atomic sites can hybridize to form bonding and antibonding 'molecular' orbitals, centred away from any individual atom[25]. In a crystal formed of these tightly bound molecular (rather than atomic) units, the valence- and conduction-band representations are induced from the (generically maximal) Wyckoff positions of the molecular orbitals, rather than from the atomic orbitals; consequently, the valence- and conduction-band Wannier functions are localized at the Wyckoff positions of the molecular orbitals, away from the atoms.

Thus, orbital hybridization, when viewed in the solid-state, represents the required transition between two atomic-limit phases with distinct symmetry. Localized, symmetric Wannier functions exist in both phases; the distinction lies in where the orbitals sit in the atomic limit[26,27]. In the first atomic limit, the orbitals lie on the atomic sites; in the second, the orbitals do not coincide with the atoms. The second phase has been called topological[28,29], but we refer to it as an 'obstructed' atomic limit because it is also described by localized Wannier states[10,30]. The prototypical example is the one-dimensional Su–Schrieffer–Heeger (Rice–Mele) chain, the two phases of which are distinguished by their hybridization pattern—an electric dipole moment that is 0 (1/2) in

the trivial (non-trivial) phase. Pumping between two different atomic limits always leads to a non-trivial cycle with observable transport quantities[31–33]. A similar phenomenon is observed in the newly discovered quadrupole insulators[34]. Signatures of the obstructed atomic limit also appear in the real-space entanglement structure of the insulating ground state in finite systems[35], and these signatures persist to systems that contain only a single molecule[36].

We now describe orbital hybridization with EBRs. The valence and conduction bands are each described by an EBR. Taken together, the two EBRs comprise a CBR. In the first and the second atomic limit, and at the critical point between them, the CBR does not change, although the individual EBRs of the valence and conduction bands do. We denote the CBR in the first atomic limit as $\sigma_v \uparrow G \oplus \sigma_c \uparrow G$, where σ_v and σ_c are irreducible representations of the site-symmetry group G_a of the atomic sites and $\uparrow$ denotes induction; the valence bands transform in the $\sigma_v \uparrow G$ band representation and the conduction bands in $\sigma_c \uparrow G$. In the second atomic limit, the CBR is $\rho_v \uparrow G \oplus \rho_c \uparrow G$, where ρ_v and ρ_c are irreducible representations of the site-symmetry group G_m of the molecular sites. As we show in Supplementary Information, a symmetry-preserving transition can happen only when the two site-symmetry groups, G_a and G_m, have a common subgroup G_0 with a representation η such that

$$\eta \uparrow G_a \approx \sigma_v \oplus \sigma_c$$
$$\eta \uparrow G_m \approx \rho_v \oplus \rho_c$$

These equations indicate that there is a line joining the atomic sites, and that Wannier functions localized along the line give the same set of bands as those localized at either endpoint. Consequently, the Wannier functions for the valence band can move from the atomic to the molecular sites while preserving all symmetries upon passing through a critical point. In Supplementary Information, we illustrate this using the example of sp orbital hybridization. We can also define an analogous notion of an obstructed atomic limit for systems that lack translational symmetry, using properties of the point group only. In this way, the preceding discussion generalizes in a straightforward manner to finite-sized crystals, molecules and even quasicrystals. In quasicrystals, obstructions to the naive atomic limit are covalent bonds. We conclude that hybridization, and therefore chemical bonding, can be treated as a phase transition.

Algorithmic materials search

We demonstrate the power of our theory by proposing two algorithms that use databases—such as the Inorganic Crystal Structure Database (ICSD; https://icsd.fiz-karlsruhe.de)—that tabulate the occupied Wyckoff positions for each element in a chemical compound, along with simple energy estimates, to identify many new classes of topological insulator and semimetal. We distinguish between the number of EBRs at the Fermi level—the two classes defined in section 'Classification of topological insulators' and summarized in Table 1. We further distinguish between cases with and without SOC, which can be treated separately using existing *ab initio* methods. The SOC strength can be viewed as a control parameter that drives the topological phase transition. For EBRs without SOC, we count bands on a per-spin basis; all states are doubly degenerate. Additional new topological semimetals, such as a series at filling −1/8, can be obtained using our method.

Single PEBRs at the Fermi level

As described in section 'Classification of topological insulators' and Table 1, a (1, 1)-type topological insulator occurs when a single PEBR is realized as a sum of two band groups disconnected in momentum space. Here, we use the fact that a large number of (1, 1)-type topological insulators can be realized by band representations induced from one-dimensional site-symmetry-group irreducible representations that are EBRs but not PEBRs. In this case, the Wannier functions for the valence band involve a single orbital per site and hence do not respect

the two-fold time-reversal-symmetry degeneracy in real space. Because the Wannier states break time-reversal symmetry, the material is necessarily a topological insulator.

An example of such a material is lead suboxide, Pb_2O (ref. 37), the topological properties of which have not previously been explored. As discussed in Supplementary Information, Pb_2O is a non-symmorphic cubic crystal in space group $Pn\bar{3}m$ (224). Although metallic, this material features a topologically disconnected PEBR far below the Fermi level (Fig. 2a). However, we can consider the application of z-axis uniaxial strain, under which the crystal symmetry is lowered to the tetragonal subgroup $P4_2/nnm$ (134) of the original space group. There are fewer symmetry constraints imposed on the band structure in this space group and, in particular, degeneracies protected by three-fold rotational symmetry will be broken. This enables a gap to open at the Fermi level, leading us to predict that strained Pb_2O will be a topological insulator with a small Fermi pocket (Fig. 2b). As an aside, we note that this analysis shows that by using group–subgroup relations we can make predictions about the topological character of strained systems when the unstrained band structure is known.

Cu_3SbS_4, a candidate topological insulator[38,39], is another example of a (1, 1)-type material. We show the calculated band structure in Fig. 2c. The states near the Fermi level form a single EBR coming from the d-orbital electrons of copper. With SOC the EBR is gapped, leading to topologically non-trivial valence and conduction bands. A trivial EBR also lies energetically within the topological gap (shown in black in the inset of Fig. 2c), which causes the effective transport gap to be smaller than the topological gap (similarly to HgTe). There are 35 additional materials in this Cu_2ABX_4 class of materials.

We use these considerations to design a systematic method to search for (1, 1)-type topological insulators. First, we identified all disconnected PEBRs using the methods described in ref. 40 and tabulated them in the BANDREP program (http://www.cryst.ehu.es/cgi-bin/cryst/programs/bandrep.pl). The PEBRs are organized by Wyckoff position and site-symmetry-group irreducible representation; in Supplementary Information we indicate which orbital types give rise to these representations. Second, we cross-reference with the ICSD, which yields a list of candidate materials. This list is further reduced by restricting to semimetals (because an insulator would not yield a topological gap near the Fermi level after turning on SOC). Last, an electron-counting analysis, using only the atomic-limit orbital energies, determines whether the topologically relevant band representations lie near the Fermi level. Carrying out this procedure led us to identify the Cu_2ABX_4 material class. We also provide a list (see Supplementary Information) of materials that are guaranteed to be semimetals by the minimal-insulator-filling criterion[41] (a sufficient, but far from necessary condition for a semimetal).

Multiple PEBRs

As described in section 'Classification of topological insulators', a CBR can be disconnected in such a way that neither the valence nor the conduction bands form PEBRs. When considering double-valued (spinful) CBRs, we classify them by whether the band representation is elementary or composite without SOC. In the first case, a single, connected, SOC-free EBR decomposes after turning on SOC into a sum of two PEBRs that are disconnected in a topologically non-trivial way. Materials with this type of topological phase transition are (1, 2)-type topological insulators. This class includes materials composed of layered Bi^{1-} square nets and related structures, which we discuss further in Supplementary Information. The relevant states at the Fermi level are the p_x and p_y orbitals of Bi, which induce a single EBR when SOC is neglected. These materials are filling-enforced semimetals with a symmetry-protected nodal (degenerate) line at the Fermi level. SOC fully gaps the nodal line, causing the EBR to disconnect. Consequently, the gap is topological. Figure 3 depicts band structures for the representative topological insulators $SrZnSb_2$ and $ZrSnTe$ (refs 42, 43).
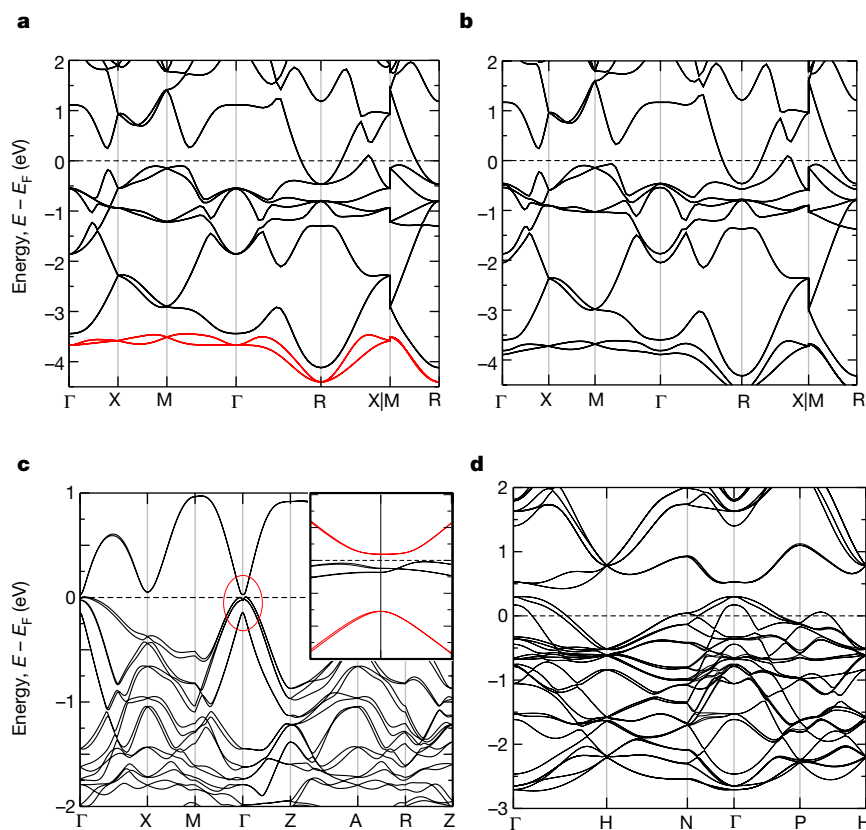
Figure 2 | Representative band structures for newly predicted materials. **a**, Band structure of Pb_2O, in space group $Pn\bar{3}m$ (224). The red group of bands about 3 eV below the Fermi level E_F originate from a topologically disconnected PEBR. **b**, Band structure for Pb_2O under uniaxial strain along the z axis. This distortion opens a topological gap near the Fermi level. **c**, Band structure for the topologically non-trivial compound Cu_3SbS_4. The conduction band, induced from a one-dimensional site-symmetry-group irreducible representation, is not a PEBR. The inset shows a close up of the gap at Γ (ringed in red), with the bands induced from conjugate one-dimensional site-symmetry-group representations highlighted in red. **d**, Band structure for the 24-fold-connected (semi-)metal Cu_3TeO_6, in space group $Ia\bar{3}$ (206). The bands at the Fermi level form a 24-band PEBR, which is half-filled.

A similar materials search program to that described in the previous subsection can be implemented for the (1, 2)-type topological insulators (Table 1). Band representations that are elementary in the absence of SOC but decompose into CBRs when SOC is turned on are quickly identified from ref. 7. With these EBRs in hand, a list of materials with the appropriate orbitals and occupied Wyckoff positions is compiled from the ICSD. Finally, an electron-counting analysis reveals which of these materials are semimetallic without SOC. The resultant materials are prime candidates for becoming topological insulators when SOC is turned on. This systematic search led us to identify more than 300 (1, 2)-type materials in space group $P4/nmm$ (129)[42–44], and 58 new

topological insulator candidates in space group $Pnma$ (62). Space group $Pnma$ (62) arises from an in-plane distortion of space group $P4/nmm$ (129), demonstrating that our group-theoretic approach enables to predict the topological character of materials upon structural distortion (see Supplementary Information).

Finally, we discuss the known topological insulators Bi_2Se_3 and KHgSb. In these materials, without SOC the band representation at the Fermi level is gapped and composite. With infinitesimal SOC, the band representation remains gapped and composite. A topological phase transition occurs only when SOC is strong enough to drive a band inversion that exchanges states with distinct little-group representations
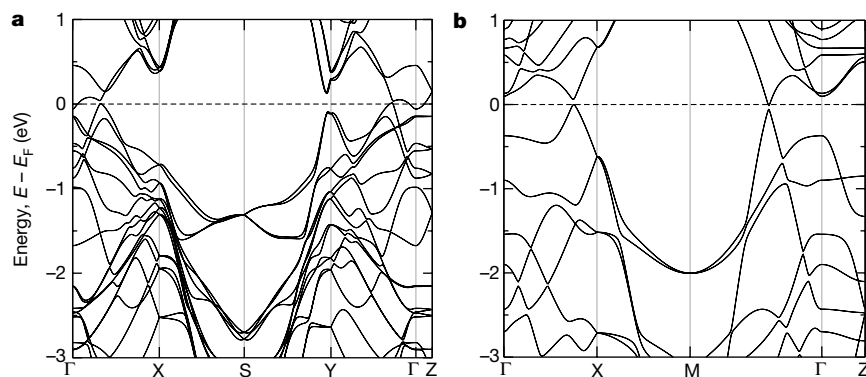

Figure 3 | Representative band structures for topologically non-trivial insulators in the Bi^{1-} square net structure type. a, Band structure of the three-dimensional weak topological insulator $SrZnSb_2$, in space group $Pnma$ (62), in which there is a small in-plane distortion in the Sb square net. **b**, Band structure of the three-dimensional weak topological insulator ZrSnTe, in space group $P4/nmm$ (129).

at Γ between the conduction and valence bands. Because such a transition depends on the strength of SOC—unlike in the (1, 1) and (1, 2) cases, for which the transition occurs at infinitesimal SOC—Bi_2Se_3 and KHgSb are described by our method, but could not be unequivocally predicted.

Partially filled bands and semimetals

Although not the main focus of this work, our method also enables the prediction of metals and semimetals. Going beyond standard methods of counting multiplicities of occupied Wyckoff positions[25], we can predict symmetry-protected semimetals by looking for partially filled, connected EBRs induced from high-dimensional site-symmetry-group representations. In this way, we found the $A_{15}B_4$ family[45] of 16-fold-connected metals in space group $I\bar{4}3d$ (220), with $A \in \{Cu, Li Na\}$ and $B \in \{Si, Ge, Sn, Pb\}$. Through charge-transfer, the 16 bands in this PEBR are 7/8 filled; this exotic filling holds promise for realizing novel physics when interactions are included. The band structure for $Li_{15}Ge_4$ is shown in Fig. 2d. There is a symmetry-protected three-fold degeneracy near the Fermi level at the P point in the Brillouin zone[46]. We calculate that Cu_3TeO_6 in space group $Ia\bar{3}$ (206)[47] has a half-filled, connected 24-band PEBR at the Fermi level when interactions are neglected. Our EBR theory reveals that this is the highest symmetry-enforced band connectivity in any space group.

Summary of systematic materials search

Although the materials presented above represent a proof-of-principle of our materials search strategy, a full, systematic search of the entire materials database using our criteria reveals many new topological insulator and semimetal candidates. Here we list some of the more promising candidate materials, verified using *ab initio* density functional theory calculations. In space group $P\bar{3}m1$ (164), we predict that $CeAl_2Ge_2$, CeISi, BiTe and Nb_3Cl_8 will be topological insulators. In space group $P4/mmm$ (123), we predict $LiBiS_2$ and $AgSbTe_2$. A particularly promising family of topological materials is given by TiAsTe, ZrSbTe, HfSbTe, $Hf_3Ni_4Ge_4$, $Sr_3Li_4Sb_4$, Ba_2Bi_3 and $Ba_3Al_2Ge_2$ in space group I/mmm (71). In addition, we identify $NaAu_2$ in space group $Fd\bar{3}m$ (227), $LaPd_2O_4$ in space group $I4_1/a$ (88), $BaGe_2Ru_2$ in space group $Fddd$ (70), $Ni_2Ta_2Te_4$ in space group $Pbam$ (53), $Ag_2Ca_4Si_6$ in space group $Fmmm$ (69), SnP in space group $I4mm$ (107) and Tl_4CuTe_3 in space group $I4/mcm$ (140), each of which we predict hosts novel topological bands.

Conclusion

We have combined group theory, chemistry and graph theory to provide a framework for topological quantum chemistry. We provide a complete description of the Wannier–Bloch duality between real and momentum space, in the process linking the extended (physics) and local (chemistry) approaches to electronic states. Our theory is descriptive and predictive: we can algorithmically search for and predict new topological insulators and semimetals. In accompanying papers[7,40], we present the data and algorithms that are necessary to derive our graph-theoretic and group-theoretic results, and to implement our materials search. By taking the ideas presented here to their logical conclusion, we arrive at a new paradigm, which applies not only to topological insulators, but also to semimetals and to band theory in general. The synthesis of symmetry and topology, of localized orbitals and Bloch wavefunctions, should enable a full understanding of non-interacting solids. Our emphasis on the symmetry of localized orbitals opens up a promising avenue to incorporating magnetic groups or interactions into the theory of topological materials.

Online Content Methods, along with any additional Extended Data display items and Source Data, are available in the online version of the paper; references unique to these sections appear only in the online paper.

Data availability All data that support the conclusions of this work are hosted on the Bilbao Crystallographic Server (http://cryst.ehu.es). All information about EBRs,

PEBRs and their connectivity graphs can be accessed via the BANDREP application (http://www.cryst.ehu.es/cgi-bin/cryst/programs/bandrep.pl). The algorithms used to generate these data, and a guide to using the relevant programs, can be found in refs 7 and 40.

1. Kittel, C. *Quantum Theory of Solids* 186–190 (Wiley, 1987).
2. Zak, J. Band representations of space groups. *Phys. Rev. B* **26**, 3010–3023 (1982).
3. Bacry, H., Michel, L. & Zak, J. in *Group Theoretical Methods in Physics* (eds Doebner, H. D. *et al.*) 289–308 (Springer, 1988).
4. Bacry, H. Duals of crystallographic groups. Band and quasi-band representations. *Commun. Math. Phys.* **153**, 359–390 (1993).
5. Evarestov, R. A & Smirnov, V. P. *Site Symmetry in Crystals* 89–184 (Springer, 1997).
6. Marzari, N., Mostofi, A. A., Yates, J. R., Souza, I. & Vanderbilt, D. Maximally localized Wannier functions: theory and applications. *Rev. Mod. Phys.* **84**, 1419–1475 (2012).
7. Elcoro, L. *et al.* Double crystallographic groups and their representations on the bilbao crystallographic server. Preproof available at https://arxiv.org/abs/1706.09272 (2017).
8. Soluyanov, A. A. & Vanderbilt, D. Wannier representation of Z_2 topological insulators. *Phys. Rev. B* **83**, 035108 (2011).
9. Soluyanov, A. A. & Vanderbilt, D. Smooth gauge for topological insulators. *Phys. Rev. B* **85**, 115415 (2012).
10. Read, N. Compactly-supported Wannier functions and algebraic *k*-theory. *Phys. Rev. B* **95**, 115309 (2017).
11. Fulton, W & Harris, J. *Representation Theory: A First Course* Ch. 3 (Springer, 2004).
12. Michel, L. & Zak, J. Elementary energy bands in crystals are connected. *Phys. Rep.* **341**, 377–395 (2001).
13. Brouder, C., Panati, G., Calandra, M., Mourougane, C. & Marzari, N. Exponential localization of Wannier functions in insulators. *Phys. Rev. Lett.* **98**, 046402 (2007).
14. Kane, C. L. & Mele, E. J. Quantum spin Hall effect in graphene. *Phys. Rev. Lett.* **95**, 226801 (2005).
15. Aroyo, M. I., Kirov, A., Capillas, C., Perez-Mato, J. M. & Wondratschek, H. Bilbao Crystallographic Server. II. Representations of crystallographic point groups and space groups. *Acta Crystallogr. A* **62**, 115–128 (2006).
16. Freed, D. S. & Moore, G. W. Twisted equivariant matter. *Ann. Henri Poincare* **14**, 1927–2023 (2013).
17. Kruthoff, J., de Boer, J., van Wezel, J., Kane, C. L. & Slager, R.-J. Topological classification of crystalline insulators through band structure combinatorics. Preprint at https://arxiv.org/abs/1612.02007 (2016).
18. Po, H. C., Vishwanath, A. & Watanabe, H. Symmetry-based indicators of band topology in the 230 space groups. Preprint at https://arxiv.org/abs/1703.00911 (2017).
19. Haldane, F. D. M. Model for a quantum Hall effect without landau levels: condensed-matter realization of the "parity anomaly". *Phys. Rev. Lett.* **61**, 2015–2018 (1988).
20. Zhang, H. *et al.* Topological insulators in Bi_2Se_3, Bi_2Te_3 and Sb_2Te_3 with a single Dirac cone on the surface. *Nat. Phys.* **5**, 438–442 (2009).
21. Xia, Y. *et al.* Observation of a large-gap topological-insulator class with a single Dirac cone on the surface. *Nat. Phys.* **5**, 398–402 (2009).
22. Winkler, G. W., Soluyanov, A. A. & Troyer, M. Smooth gauge and wannier functions for topological band structures in arbitrary dimensions. *Phys. Rev. B* **93**, 035453 (2016).
23. Liu, Z. *et al.* A stable three-dimensional topological dirac semimetal Cd_3As_2. *Nat. Mater.* **13**, 677–681 (2014).
24. Liu, Z. *et al.* Discovery of a three-dimensional topological dirac semimetal, Na_3Bi. *Science* **343**, 864–867 (2014).
25. Hoffmann, R. How chemistry and physics meet in the solid state. *Angew. Chem. Int. Edn Engl.* **26**, 846–878 (1987).
26. Zak, J. Berry's phase for energy bands in solids. *Phys. Rev. Lett.* **62**, 2747–2750 (1989).
27. King-Smith, R. D. & Vanderbilt, D. Theory of polarization of crystalline solids. *Phys. Rev. B* **47**, 1651(R)–1654(R) (1993).
28. Ryu, S. & Hatsugai, Y. Topological origin of zero-energy edge states in particle-hole symmetric systems. *Phys. Rev. Lett.* **89**, 077002 (2002).
29. Bernevig, B. A & Hughes, T. L. *Topological Insulators and Topological Superconductors* 226–228 (Princeton Univ. Press, 2013).
30. Kivelson, S. Wannier functions in one-dimensional disordered systems: application to fractionally charged solitons. *Phys. Rev. B* **26**, 4269–4277 (1982).
31. Rice, M. J. & Mele, E. J. Elementary excitations of a linearly conjugated diatomic polymer. *Phys. Rev. Lett.* **49**, 1455–1459 (1982).
32. Atala, M. *et al.* Direct measurement of the Zak phase in topological bloch bands. *Nat. Phys.* **9**, 795–800 (2013).
33. Nakajima, S. *et al.* Topological Thouless pumping of ultracold fermions. *Nat. Phys.* **12**, 296–300 (2016).
34. Benalcazar, W. A., Bernevig, B. A. & Hughes, T. L. Quantized electric multipole insulators. Preprint at https://arxiv.org/abs/1611.07987 (2016).
35. Fang, C., Gilbert, M. J. & Bernevig, B. A. Entanglement spectrum classification of C_n-invariant noninteracting topological insulators in two dimensions. *Phys. Rev. B* **87**, 035119 (2013).

36. Tubman, N. M. & Yang, D. C. Quantum dissection of a covalent bond with the entanglement spectrum. Preprint at https://arxiv.org/abs/1412.1495 (2014).
37. Ferrari, A. Il sottossido di piombo. *Gazz. Chim. Ital.* **56,** 630 (1926).
38. Pfitzner, A. & Reiser, S. Refinement of the crystal structures of Cu_3Ps_4 and Cu_3SbS_4 and a comment on normal tetrahedral structures. *Z. Kristallogr.* **217,** 51 (2002).
39. Wang, Y., Lin, H., Das, T., Hasan, M. & Bansil, A. Topological insulators in the quaternary chalcogenide compounds and ternary famatinite compounds. *New J. Phys.* **13,** 085017 (2011).
40. Vergniory, M. G. *et al.* Graph theory data for topological quantum chemistry. Preproof available at https://arxiv.org/abs/1706.08529 (2017).
41. Watanabe, H., Po, H. C., Zaletel, M. P. & Vishwanath, A. Filling-enforced gaplessness in band structures of the 230 space groups. *Phys. Rev. Lett.* **117,** 096404 (2016).
42. Xu, Q. *et al.* Two-dimensional oxide topological insulator with iron-pnictide superconductor lifeas structure. *Phys. Rev. B* **92,** 205310 (2015).
43. Lou, R. *et al.* Emergence of topological bands on the surface of zrsnte crystal. *Phys. Rev. B* **93,** 241104(R) (2016).
44. Schoop, L. M. *et al.* Dirac cone protected by non-symmorphic symmetry and three-dimensional Dirac line node in ZrSiS. *Nat. Commun.* **7,** 11696 (2016).
45. Morris, A. J., Grey, C. P. & Pickard, C. J. Thermodynamically stable lithium silicides and germanides from density functional theory calculations. *Phys. Rev. B* **90,** 054111 (2014).
46. Bradlyn, B. *et al.* Beyond Dirac and Weyl fermions: unconventional quasiparticles in conventional crystals. *Science* **353,** aaf5037 (2016).
47. Falck, L., Lindqvist, O. & Moret, J. Tricopper(II) tellurate(VI). *Acta Crystallogr. B* **34,** 896–897 (1978).

Supplementary Information is available in the online version of the paper.

Author Contributions B.B., J.C., Z.W. and B.A.B. provided the theoretical analysis, with input from C.F. J.C. developed specific models to test the theory. L.E. and M.I.A. performed the computerized group-theoretic computations. B.B., L.E. and M.G.V. devised and developed the graph algorithms and the EBR connectivities; L.E. and M.G.V. performed the computerized graph-theory computations. Z.W. discovered the new materials presented here with input from C.F., and performed all of the first-principles calculations.

Author Information Reprints and permissions information is available at www.nature.com/reprints. The authors declare no competing financial interests. Readers are welcome to comment on the online version of the paper. Publisher's note: Springer Nature remains neutral with regard to jurisdictional claims in published maps and institutional affiliations. Correspondence and requests for materials should be addressed to B.A.B. (bernevig@princeton.edu).